

Discovering Modes of Action for Therapeutic Compounds Using a Genome-Wide Screen of Yeast Heterozygotes

Pek Yee Lum,^{1,6,*} Christopher D. Armour,^{1,6}
Sergey B. Stepaniants,¹ Guy Cavet,¹
Maria K. Wolf,³ J. Scott Butler,³ Jerald C. Hinshaw,⁵
Philippe Garnier,⁵ Glenn D. Prestwich,⁵
Amy Leonardson,¹ Philip Garrett-Engele,¹
Christopher M. Rush,⁴ Martin Bard,⁴
Greg Schimmack,¹ John W. Phillips,²
Christopher J. Roberts,¹ and Daniel D. Shoemaker¹

¹Rosetta Inpharmatics LLC, a wholly-owned subsidiary of Merck & Co., Inc.

12040 115th Avenue N.E.
Kirkland, Washington 98034

²Merck & Co., Inc.
126 East Lincoln Avenue
R80Y-255

Rahway, New Jersey 07065

³Department of Microbiology and Immunology
J.P. Wilmot Cancer Center
University of Rochester School of Medicine and
Dentistry

601 Elmwood Avenue
Rochester, New York 14642

⁴Department of Biology
Indiana University-Purdue University Indianapolis
723 West Michigan Street
Indianapolis, Indiana 46202

⁵Department of Medicinal Chemistry
The University of Utah
419 Wakara Way, Suite 205
Salt Lake City, Utah 84108

Summary

Modern medicine faces the challenge of developing safer and more effective therapies to treat human diseases. Many drugs currently in use were discovered without knowledge of their underlying molecular mechanisms. Understanding their biological targets and modes of action will be essential to design improved second-generation compounds. Here, we describe the use of a genome-wide pool of tagged heterozygotes to assess the cellular effects of 78 compounds in *Saccharomyces cerevisiae*. Specifically, lanosterol synthase in the sterol biosynthetic pathway was identified as a target of the antianginal drug molsidomine, which may explain its cholesterol-lowering effects. Further, the rRNA processing exosome was identified as a potential target of the cell growth inhibitor 5-fluorouracil. This genome-wide screen validated previously characterized targets or helped identify potentially new modes of action for over half of the compounds tested, providing proof of this principle for

analyzing the modes of action of clinically relevant compounds.

Introduction

The sequencing of the human genome has revealed thousands of putative proteins that have the potential to revolutionize modern medicine (Lander et al., 2001). A critical step in translating genomic information into new therapeutics will be to develop approaches that can rapidly distinguish high-quality drug targets among the thousands of potential candidates. Identifying the cellular targets of clinically proven small molecules is a powerful approach to identify proteins that can be safely and effectively targeted in humans. Interestingly, many of the therapeutic compounds on the market today were discovered fortuitously with no a priori knowledge of the target or mechanism of action. For example, the beneficial effects of niacin on lipid levels in humans have been known since 1955, while identification of its cellular target remained elusive until just recently (Knopp, 1999; Tunaru et al., 2003). The importance of the identification of the target of a clinically proven molecule such as niacin shows that these molecules provide a rich source of chemical probes that can be used to mine the human genome for the next generation of high-quality drug targets.

A major challenge facing this type of approach is the need for new tools that can rapidly identify the protein targets of small molecules with interesting biological properties. The emergence of new technologies such as protein arrays (MacBeath and Schreiber, 2000; Service, 2000), reverse transfection (Phizicky et al., 2003; Ziauddin and Sabatini, 2001), and DNA microarrays (Huels et al., 2002) has accelerated this type of discovery effort. Model organisms such as *Saccharomyces cerevisiae* have also proven to be powerful tools for mechanistic studies of clinically relevant compounds (Heitman et al., 1991; Schreiber and Crabtree, 1992), which is made possible by the fact that many human disease-associated genes have highly conserved yeast counterparts (Foury, 1997; Steinmetz et al., 2002).

A study by Giaever et al. (1999) demonstrated that parallel analysis of yeast strains with heterozygous deletions of drug target genes can be used to monitor compound activities in vivo. Specifically, they showed that reducing the gene copy number of drug targets in a diploid cell can result in sensitization to the drug of interest. We have extended this approach to analyze the activities of 78 chemical entities, most of which are medically relevant. In addition, we increased the number of mutant strains to represent over half of the yeast genome and used high-density oligonucleotide arrays with a two-color labeling strategy to monitor growth rates. Finally, a strain-specific error model was used to identify drug-dependent fitness defects that are statistically significant. In this study, we correctly identified the reported targets for many well-characterized com-

*Correspondence: pek_lum@merck.com; shoemakd@stanford.alumni.org

⁶These authors contributed equally to this work

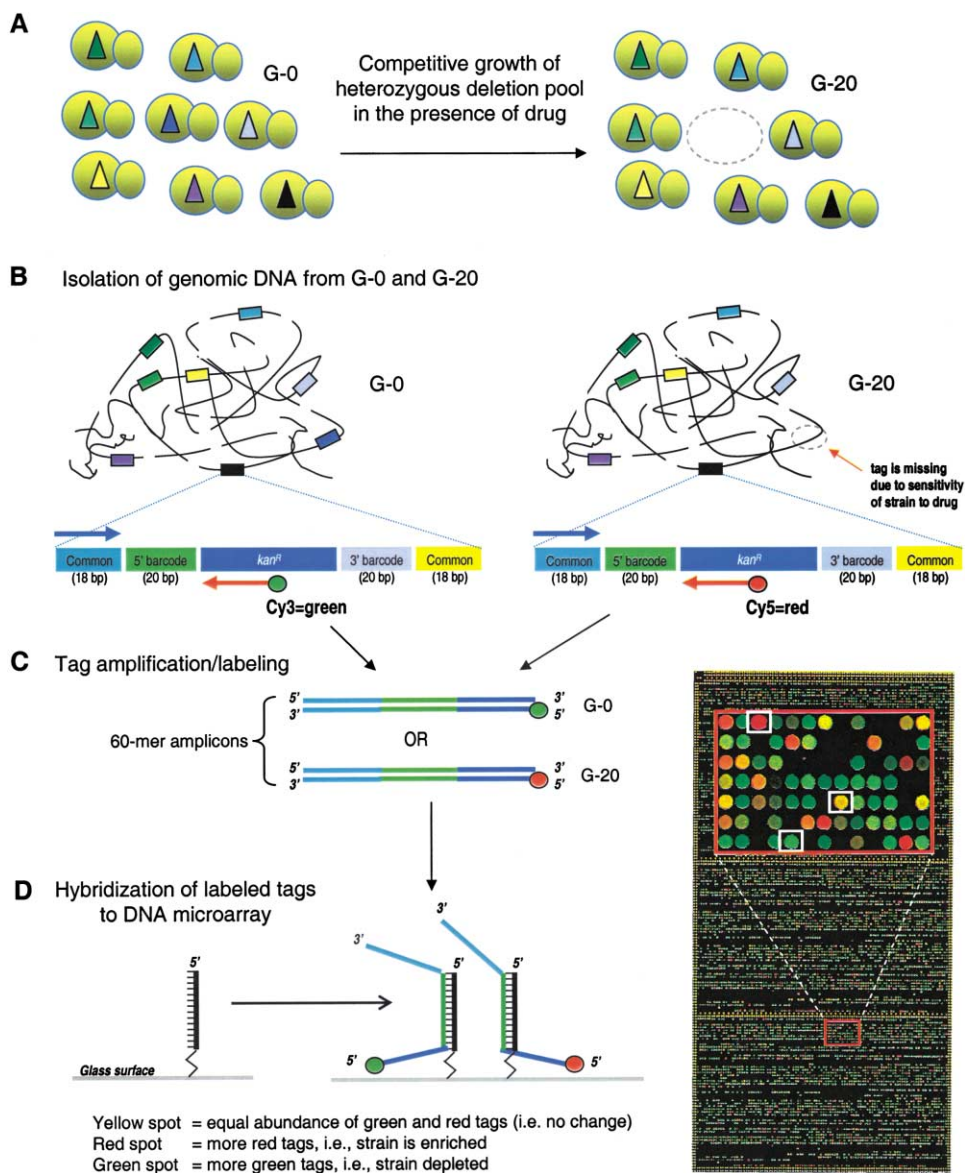


Figure 1. Schematic Representation of the Fitness Profiling Experimental Strategy

(A) Growth of tagged heterozygous deletion pool grown in the presence of drug.

(B) Isolation of genomic DNA from cultures before (G-0) and after (G-20) outgrowth.

(C) Amplification and labeling of barcode tags by PCR.

(D) Hybridization of labeled barcode tags to DNA microarrays. Signal intensities resulting from microarray hybridizations are proportional to the relative tag abundances in the pool population. The inset shows an enlargement of a microarray following hybridization with examples of an enriched strain (red spot), a depleted strain (green spot), and a strain that was unchanged (yellow spot).

pounds in addition to discovering many potentially novel drug targets.

Results

Study Design Rationale

The experimental strategy used to interrogate drug activities in this study is outlined in Figure 1. A mixture of isogenic yeast mutants was generated by pooling 3503 heterozygous deletion strains engineered with strain-specific molecular barcode tags (see Experimental Pro-

cedures). Competitive growth of the mutant pool was carried out for 20 generations in media containing selected compounds (Figure 1A). Strain abundance was measured before and after outgrowth by hybridization of differentially labeled (Cy3/Cy5) barcode tags to DNA microarrays (Figures 1B–1D). Deletion strains that were sensitive to a given compound were outcompeted by thousands of unaffected strains in the pool. Compounds were administered at concentrations resulting in moderate growth inhibition to ensure that the activities of the putative drug target(s) were rate limiting for growth. Un-

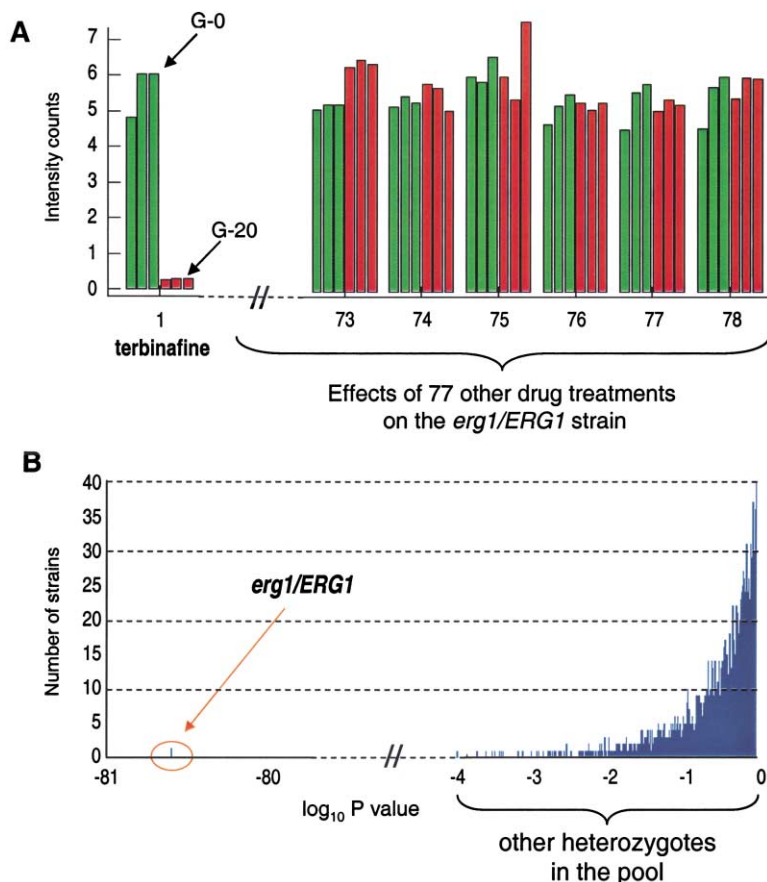


Figure 2. Identification of Drug-Specific Growth Defects

(A) Compilation of signal intensity data for the *ERG1* heterozygote barcode tag across all 78 drug treatments. The Cy3 (green) or Cy5 (red) signal intensities were obtained from tag-specific oligonucleotide features represented in triplicate on the microarray. In most drug treatments, the Cy3 and Cy5 intensities were roughly equal indicating that the strain abundance remained unchanged over the course of most drug treatments. In the terbinafine treatment, however, the Cy5 intensity is much lower than that of the Cy3 for the *ERG1* heterozygote tag. This indicates that the relative abundance of the *ERG1* heterozygote was depleted during outgrowth in the presence of terbinafine, which is known to inhibit Erg1p activity.

(B) Statistical significance of terbinafine-specific fitness changes in the pool. Hybridization data across all drug treatments were used to determine the average performance of each strain during outgrowth. A modified Student's *t* test was used to calculate confidence levels by comparing the fitness levels from individual treatments to the average performance across all treatments. The resulting P values for each strain in the terbinafine treatment are plotted on the x axis and the number of strains with a given P value are plotted on the y axis. Notice that the *erg1/ERG1* strain is the single outlier in the terbinafine treatment.

der these conditions, strains that are heterozygous for drug target genes have the greatest chance of displaying hypersensitivity phenotypes (Giaever et al., 1999).

Identifying Drug-Specific Growth Defects

A strain-specific error model was developed to distinguish between general and drug-dependent growth defects. To accomplish this, a reference set was generated by calculating the mean performance of each strain across a large number of competitive growth experiments. Next, the scatter error for these measurements was calculated to determine the reproducibility of each strain's performance. To identify strains with drug-specific changes in growth rates, the fitness values from a given drug treatment were compared to the corresponding values in the reference set using a modified Student's *t* test (see Experimental Procedures). The resulting P values reflect the probability that the observed growth rate in any given drug treatment could occur by chance based on the strain's behavior in the reference set.

Figure 2A shows an example of the hybridization data collected for one of the heterozygotes (*ERG1*) before (Cy3) and after (Cy5) each of the 78 different competitive growth experiments. The 20 bp tags for each of the strains in the pool were printed in triplicate on the microarrays that were used for these experiments. In this example, the relative growth rate of the *ERG1* heterozygote was not affected by the majority of the drug treat-

ments as indicated by the similarity of hybridization intensities before and after each of the competitive growth experiments. However, the \log_{10} intensities of the amplified tags showed a significant reduction following treatment with terbinafine suggesting that the *erg1/ERG1* strain had been depleted from the population. Figure 2B shows the results of \log_{10} P values for all 3503 strains in the pool following terbinafine treatment. The *ERG1* heterozygote was the most significant outlier with a P value of less than 1×10^{-85} .

Large-Scale Analysis of 78 Compounds

This screen was initiated by testing commercially available compounds for the ability to inhibit growth in our yeast strain background (see Experimental Procedures for description). Seventy-eight compounds that induced moderate levels of growth inhibition ($0.70 \leq$ pool fitness ≤ 0.96 ; see Experimental Procedures for definition of pool fitness) were selected for analysis (Table 1). The compounds analyzed in this study included many clinically used therapeutic agents and agricultural chemicals. Figure 3 shows an overview of the P value data for all 3503 strains across the 78 compound treatments (also in Supplemental Table S1 available at <http://www.cell.com/cgi/content/full/116/1/121/DC1>). Of the 78 compounds analyzed, 18 resulted in no drug-specific fitness changes (Group I), 56 resulted in a small number of significant outliers (Group II), and 4 resulted in widespread fitness changes (Group III) compared to the refer-

Table 1. A Compendium of 78 Compounds

CAS Number ^a	Compound Name	Clinical Indication ^b	Regulatory Status ^c	Dose Tested	Pool Fitness	Significant Outlier Strains	Reported Target(s)
2022-85-7	5-Fluorocytosine (5FC)	antifungal	FDA-approved	200 ng/mL	0.80	RRP6 (-20.69), NOP4 (-20.08), YPR143W (-12.42)	CDC21 (Hardman et al., 2001)
50-91-9	5-Fluorodeoxyuridine (FUdR)	antiviral; antineoplastic	FDA-approved	300 μ M	0.81	RRP6 (-16.21), HOF1 (-13.34), RSB1 (-10.65)	CDC21 (Hardman et al., 2001)
51-21-8	5-Fluorouracil (5FU)	antineoplastic	FDA-approved	2 μ M	0.92	RRP6 (-17.79), RRP41 (-15.9), MAK21 (-12.1)	CDC21 (Hardman et al., 2001)
50-76-0	Actinomycin D	antineoplastic	FDA-approved	20 μ g/mL	0.72	VMA21 (-138.66), YOR114W (-115.57), PRP28 (-95.23)	
50-48-6	Amitriptyline	antidepressant	FDA-approved	125 μ g/mL	0.77	GFA1 (-68.37), NEO1 (-31.1), YKL111C (-29.7)	
1397-89-3	Amphotericin B	antifungal	FDA-approved	600 ng/mL	0.89	ACC1 (-10.65), YSH1 (-8.94), THS1 (-6.77)	
147-94-4	Ara-CMP	antineoplastic	not listed	500 μ g/mL	0.88	SHY1 (-46.98), YGR122W (-35.73), AVT2 (-32.98)	
3337-71-1	Asulam	herbicide	not listed	250 μ g/mL	0.95	FOL2 (-26.16), CDC21 (-12.18), GIC2 (-3.69)	FOL1, FOL3 (Nardese et al., 1996; Patel et al., 2003)
29122-68-7	Atenolol	antihypertensive, antianginal, antiarrhythmic	FDA-approved	4.0 mg/mL	0.90	POP3 (-6.16), RIT1 (-5.66), TRK1 (-4.21)	
30516-87-1	Azidothymidine (AZT)	antiviral	FDA-approved	2.0 mg/mL	0.96	YDR230W (-3.64), CDC26 (-3.45), YHR029C (-3.32)	
not listed	Benoxinate	local anesthetic	not listed	900 μ g/mL	0.83	ERG7 (-14.46), ROX3 (-11.02), CIS3 (-5.03)	
58-08-2	Caffeine	CNS stimulant; respiratory stimulant	FDA-approved	700 μ g/mL	0.71	KOG1 (-68.88), TOR1 (-46.97), SHD7 (-24.4)	
7689-03-4	Camptothecin	antineoplastic	not listed	100 μ g/mL	0.96	TRX2 (-11.7), YPL251W (-6.77), YLR003C (-6.06)	TOP1 (Pommier et al., 1998)
10605-21-7	Carbendazim	fungicide	not listed	100 μ g/mL	0.81	GIM2 (-109.06), GIM3 (-90.46), CLN2 (-75.36)	TUB/TUB2 (Geissler et al., 1998; Neff et al., 1983)
50-53-3	Chlorpromazine	antiemetic; antipsychotic	FDA-approved	37.5 μ g/mL	0.93	DOP1 (-23.27), NEO1 (-21.76), KRE25 (-15.71)	
15663-27-1	Cisplatin	antineoplastic	FDA-approved	600 μ M	0.88	VPS65 (-6.38), PSY2 (-5.23), ATP4 (-4.32)	
303-49-1	Clomipramine	antidepressant; antiobsessional agent	FDA-approved	50 μ g/mL	0.88	NEO1 (-32.91), YFR044C (-20.53), CAN1 (-14.69)	
23593-75-1	Clotrimazole	antifungal	FDA-approved	37.5 ng/mL	0.85	PDR16 (-46.66), ERG11 (-46.33), PDR5 (-21.49)	ERG11 (Truan et al., 1994)
66-81-9	Cycloheximide	fungicide; plant growth regulator	not listed	10 ng/mL	0.90	RPP0 (-9.3), CIS3 (-4.3), NIPI100 (-4.01)	RPL41A/RPL41B (Stocklein and Piepersberg, 1980)
57966-95-7	Cymoxanil	agricultural fungicide	not listed	1.25 μ g/mL	0.90	LCB1 (-16.62), YBR226C (-9.39), URA1 (-6.53)	
20830-81-3	Daunorubicin	antineoplastic	FDA-approved	40 ng/mL	0.96	LSM6 (-11.48), PLO2 (-8.56), BSC2 (-8.55)	
50-47-5	Desipramine	antidepressant	FDA-approved	200 μ g/mL	0.87	NEO1 (-33.23), GOS1 (-17.34), KES1 (-8.58)	

(continued)

Table 1. Continued

CAS Number ^a	Compound Name	Clinical Indication ^b	Regulatory Status ^c	Dose Tested	Pool Fitness	Significant Outlier Strains	Reported Target(s)
42399-41-7	Diltiazem	antihypertensive; antiarrhythmic	FDA-approved	2.0 mg/mL	0.86	YMR187C (-4.39), YLR016C (-3.97), PMT3 (-3.19)	
67-68-5	Dimethylsulfoxide (DMSO)	not listed	FDA-approved	2.5%	0.93	CDC31 (-32.03), YOR256C (-16.55), YOR356W (-9.53)	
23214-92-8	Doxorubicin	antineoplastic	FDA-approved	3 µg/mL	0.91	GIC2 (-16.31), YDR319C (-13.8), MIG2 (-13.78)	
564-25-0	Doxycycline	antibacterial	FDA-approved	400 µg/mL	0.86	ERV1 (-9.63), SDS3 (-6.88), SRB5 (-5.24)	
586-60-7	Dyclonine	local anesthetic	FDA-approved	32 µg/mL	0.85	ERG2 (-13.16), RPS24A (-3.01), SSA2 (-2.55)	ERG2 (Hughes et al., 2000)
not listed	Efavirenz	antiviral	FDA-approved	300 µg/mL	0.91	YBL086C (-3.75), YKR065C (-3.67), SCW10 (-3.28)	
1264-62-6	Erythromycin Ethylsuccinate	antibacterial	FDA-approved	2.5 mg/mL	0.89	YOR1 (-21.43), YGL069C (-11.15), SEC17 (-9.28)	
64-17-5	Ethanol	not listed	FDA-approved	1.25%	0.79	CMK1 (-5.7), MLH1 (-5.53), DPM1 (-4.91)	
67306-03-0	Fenpropimorph	systemic fungicide	not listed	0.00001%	0.82	ERG2 (-18.55), ISW1 (-4), BZZ1 (-3.42)	ERG2 (Marcireau et al., 1990)
5104-49-4	Flurbiprofen	anti-inflammatory; analgesic	FDA-approved	75 µg/mL	0.83	YCR016W (-7.89), SEC10 (-6.73), ATP4 (-6.24)	
25812-30-	Gemfibrozil	antihyperlipoproteinemic	FDA-approved	30 µg/mL	0.75	SPC19 (-12.06), YNL179C (-8.31), SEC13 (-7.05)	
67-99-2	Gliotoxin	not listed	not listed	3.0 µg/mL	0.91	ACC1 (-6.98), YMR306C-A (-3.78), ERG28 (-3.54)	
52-86-8	Haloperidol	antidyskinetic; antipsychotic	FDA-approved	62.5 µg/mL	0.85	SET6 (-59.45), ERG3 (-33.89), OLE1 (-25.58)	ERG2 (Moebius et al., 1996)
51-45-6	Histamine	not listed	FDA-approved	3 mg/mL	0.80	YGL042C (-21.31), LOT6 (-8.76), YLR164W (-8.69)	
127-07-1	Hydroxyurea	antineoplastic; treatment of sickle cell anemia	FDA-approved	20 mM	0.91	RNR4 (-12.2), RNR2 (-8.29), RMS1 (-7.04)	RNR2, RNR4 (Rittberg and Wright, 1989)
15687-27-1	Ibuprofen	anti-inflammatory; analgesic; antipyretic	FDA-approved	10 µg/mL	0.92	BCP1 (-4.26), YIR024C (-3.94), UBA2 (-3.25)	
50-49-7	Imipramine	antidepressant	FDA-approved	312.5 µg/mL	0.74	DOP1 (-67.37), KRE25 (-31.89), YKL111C (-30.7)	
53-86-1	Indomethacin	anti-inflammatory, antipyretic, analgesic	FDA-approved	100 µg/mL	0.85	FAS1 (-117.96), LCB2 (-28.26), YPL272C (-23.41)	
54-85-3	Isoniazid	tuberculostatic antibacterial	FDA-approved	275 µg/mL	0.89	HSP82 (-9.09), YMR158W-A (-9.07), RSC2 (-8.66)	
8063-07-8	Kanamycin	antibacterial	FDA-approved	6.0 mg/mL	0.95	ZIP1 (-4.18), YPR152C (-3.23), YNL184C (-2.59)	
75330-75-5	Lovastatin	antihyperlipoproteinemic	FDA-approved	40 µg/mL	0.80	HMG1 (-9.54), VPS8 (-5.29), YPL197C (-2.24)	HMG1/HMG2 (Rine et al., 1983)
58-27-5	Menadione	prothrombogenic vitamin	FDA-approved	40 ng/mL	0.80	GIM1 (-14.59), RPN10 (-6.91), YDR107C (-6.08)	

(continued)

Table 1. Continued

CAS Number ^a	Compound Name	Clinical Indication ^b	Regulatory Status ^c	Dose Tested	Pool Fitness	Significant Outlier Strains	Reported Target(s)
59-05-2	Methotrexate	antineoplastic; antirheumatic	FDA-approved	12.5 µg/mL	0.90	CIN1 (-9.7), YMR247C (-6.16), SPP1 (-5.91)	DFR1 (Huang et al., 1992)
66-27-3	Methyl Methanesulfonate (MMS)	experimental mutagen, teratogen, carcinogen	not listed	0.002%	0.84	HEM2 (-39.97), HEM1 (-27.12), KRE21 (-14.44)	
364-62-5	Metoclopramide	antiemetic	FDA-approved	7.0 mg/mL	0.88	GFA1 (-74.5), HIP1 (-22.44), YGR190C (-20.03)	
25717-80-0	Molsidomine	antianginal	not listed	2.0 mg/mL	0.84	ERG7 (-16.08), QCR10 (-5.15), YPL071C (-4.65)	
389-08-2	Nalidixic acid	antibacterial	FDA-approved	325 µg/mL	0.88	YLR312C (-15.83), RIT1 (-13.07), NAM8 (-11.51)	
22204-53-1	Naproxen	anti-inflammatory; analgesic; antipyretic	FDA-approved	40 µg/mL	0.93	YPR148C (-4.31), YLR402W (-4.25), RIB5 (-4.1)	
129618-40-2	Nevirapine	antiviral	FDA-approved	250 µg/mL	0.96	YPL103C (-5.58), RIM21 (-5.48), YDR314C (-5.28)	
55985-32-5	Nicardipine	antianginal; antihypertensive	FDA-approved	1.0 mg/mL	0.93	GFA1 (-67.99), YPL238C (-4.24), HIP1 (-3.9)	
21829-25-4	Nifedipine	antianginal; antihypertensive; antibacterial	FDA-approved	200 µg/mL	0.83	PM1C1 (-4.82), AAD6 (-3.7), PPE1 (-3.54)	
67-20-9	Nitrofurantoin	antibacterial	FDA-approved	500 µg/mL	0.78	YLR022C (-3.31), FRT1 (-3.17), YLR241W (-2.96)	
73590-58-6	Omeprazole	antilulcerative	FDA-approved	50 µg/mL	0.82	YNL184C (-4.68), YPL206C (-4.55), GCR1 (-4.51)	PMA1 (Monk et al., 1995)
7542-37-2	Paromomycin	antibacterial; antiamebic	FDA-approved	5.0 mg/mL	0.95	SSS1 (-4.85), RPS13 (-1.92), MRP21 (-1.79)	
100-33-4	Pentamidine	antiprotozoal; antipneumocystic	FDA-approved	250 µg/mL	0.90	CDH1 (-43.04), SDH3 (-38.56), MRP13 (-35.78)	
50-33-9	Phenylbutazone	anti-inflammatory	FDA-discontinued	200 µg/mL	0.89	YOR356W (-4.74), HIR1 (-3.08), YDR051C (-2.85)	
140-65-8	Pramoxine	local anesthetic	FDA-approved	16 µg/mL	0.84	ERG2 (-7.22), STB1 (-3.9), BZZ1 (-3.63)	
59-46-1	Procaine	local anesthetic	FDA-approved	2.5 mg/mL	0.90	GFA1 (-44.61), HIP1 (-29.93), YGR190C (-25.53)	
60-87-7	Promethazine	antihistaminic	FDA-approved	100 µg/mL	0.92	NEO1 (-15.92), YOR263C (-6.78), FTH1 (-6.61)	
7784-46-5	Sodium Arsenite	topical acaricide	not listed	20 µg/mL	0.89	TRK1 (-11.03), RIT1 (-7.45), GCD2 (-6.4)	
7647-14-5	Sodium Chloride	not listed	not listed	250 mM	0.89	YBL086C (-13.74), YDR049W (-9.98), GPI1 (-8.5)	
13755-38-9	Sodium Nitroprusside	antihypertensive	FDA-approved	667 µg/mL	0.89	HEM1 (-36.27), NNT1 (-11.16), YLR280C (-9.62)	
62996-74-1	Staurosporine	antibacterial	not listed	2.0 mg/mL	0.95	RHO1 (-58.62), CDC12 (-41.54), ROT1 (-22.28)	PKC1 (Yoshida et al., 1992)

(continued)

Table 1. Continued

CAS Number ^a	Compound Name	Clinical Indication ^b	Regulatory Status ^c	Dose Tested	Pool Fitness	Significant Outlier Strains	Reported Target(s)
723-46-6	Sulfamethoxazole	antibacterial; antipneumocystic	FDA-approved	200 µg/mL	0.85	FOL2 (-49.11), MET12 (-20.85), CDC21 (-18.97)	FOL1, FOL3 (Nardese et al., 1996; Patel et al., 2003)
63-74-1	Sulfanilamide	antibacterial	FDA-approved	625 µg/mL	0.86	FOL2 (-37.42), CDC21 (-19.53), YBL073W (-16.65)	FOL1, FOL3 (Nardese et al., 1996; Patel et al., 2003)
57-96-5	Sulfinpyrazone	uricosuric; antithrombotic	FDA-approved	20 µg/mL	0.92	FAS1 (-29.37), RIT1 (-9.56), TIM18 (-7.42)	
74222-97-2	Sulfometuron-methyl	herbicide	not listed	1.25 µg/mL	0.90	YOR286W (-11.65), YPL267W (-6.52), YPL272C (-6.17)	
10540-29-1	Tamoxifen	antiestrogen; hormonal antineoplastic	FDA-approved	3.5 µg/mL	0.86	NEO1 (-31.44), GCD2 (-5.2), YNL179C (-5.18)	
78628-80-5	Terbinafine	antibacterial	FDA-approved	2.5 µg/mL	0.89	ERG1 (-80.59), YGR176W (-16.1), NCP1 (-8.64)	ERG1 (Jandrositz et al., 1991)
60-54-8	Tetracycline	antibacterial	FDA-approved	800 µg/mL	0.96	RIM2 (-19.18), RPD3 (-13.69), SLS1 (-8.84)	
50-35-1	Thalidomide	immunomodulator	FDA-approved	1.0 mg/mL	0.93	YOR318C (-3.6), YOR170W (-3.28), YOL083W (-3.19)	
117-89-5	Trifluoperazine	antipsychotic	FDA-approved	17.5 µg/mL	0.91	NEO1 (-31.74), NOC2 (-5.82), YDR339C (-4.76)	
97322-87-7	Troglitazone	antidiabetic	FDA-discontinued	300 µg/mL	0.89	POP3 (-5), PPT1 (-3.49), YEL001C (-3.48)	
11089-65-9	Tunicamycin	antibiotic used in glycoprotein research	not listed	150 ng/mL	0.83	YFL032W (-67.77), ALG7 (-24), GFA1 (-23.81)	ALG7 (Barnes et al., 1984)
99-66-1	Valproic Acid	anticonvulsant; antimanic; antimigraine	FDA-approved	300 µg/mL	0.94	CIS3 (-3.01), YOL075C (-2.73), HCS1 (-2.18)	
81-81-2	Warfarin	anticoagulant	FDA-approved	500 µg/mL	0.85	YEN1 (-7.75), BUL1 (-6.62), RIT1 (-5.49)	

The table lists each compound that was analyzed in this study. The clinical indication (Merck Index, Thirteenth Edition), regulatory status (FDA Orange Book, 15 Sept, 2003), dose tested, pool fitness level are provided for each compound. In addition, the three most significant outlier strains with log₁₀ P values (parentheses) are listed from left to right in order of significance. Reported drug targets are accompanied by relevant literature citations.

^aCAS Registry; September 15, 2003

^bThe Merck Index, Thirteenth Edition

^cFDA Orange Book: <http://www.fda.gov/cder/ob/default.htm> (15 September, 2003)

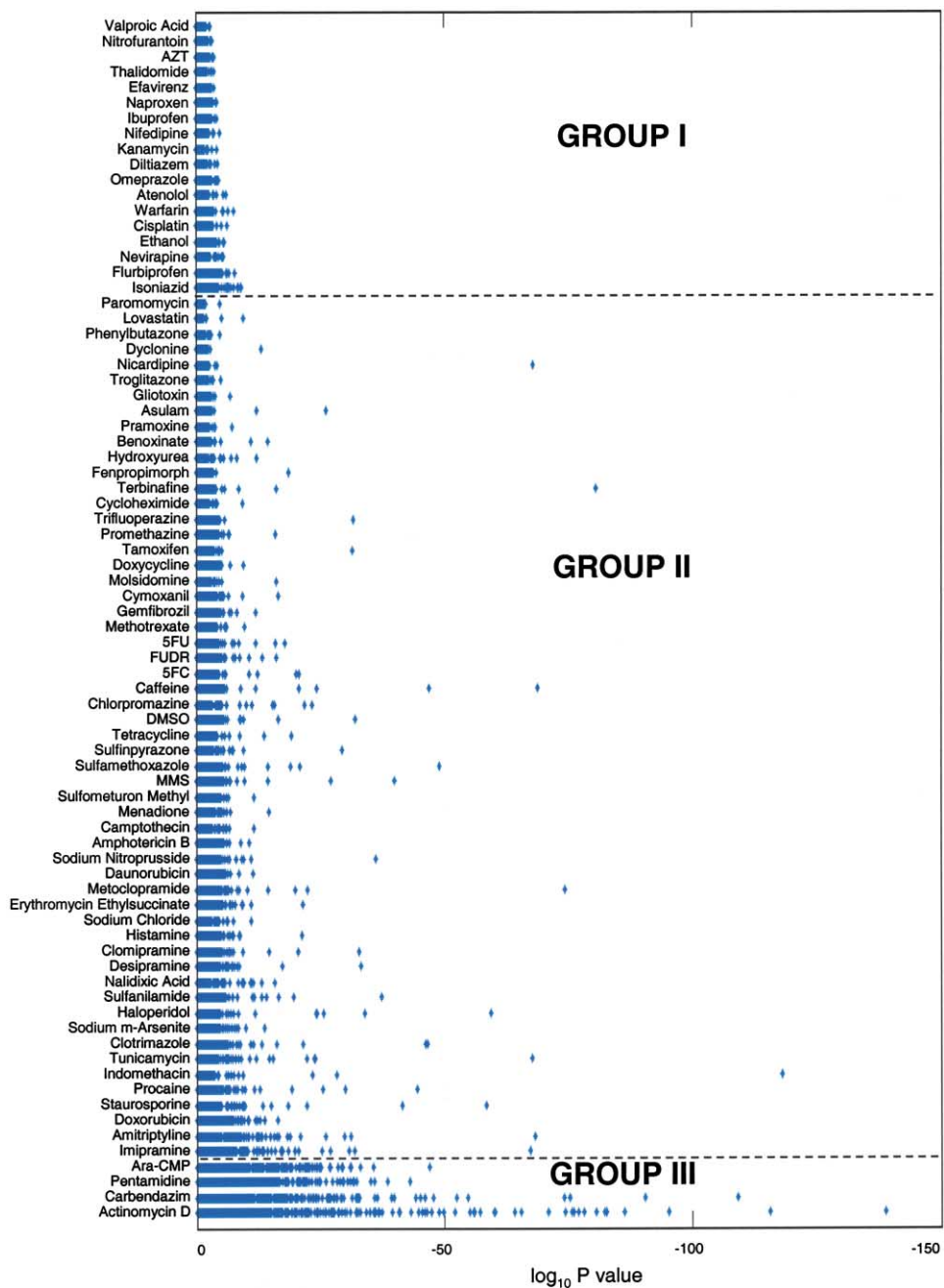


Figure 3. Comprehensive View of Fitness Profiles for 78 Compounds

Dot plots were calculated by comparing drug-specific growth rates of each heterozygous deletion strain to its average behavior from the reference set. Statistical significance was determined for each strain's fitness value and the resulting P values were plotted for strains with drug-specific growth deficits. Each data point represents one heterozygous deletion strain with a growth deficit. The confidence level of each strain's growth rate is plotted along the x axis as the \log_{10} P value. The P value distributions are most useful for identifying outlier strains within drug treatments. Compounds are sorted by the overall distribution of the heterozygous deletion pool with compounds causing relatively few fitness changes at the top and those causing widespread fitness changes at the bottom. Group I includes compounds with no drug-specific fitness changes. Compounds in Group II resulted in a small number of highly significant outliers. Group III compounds induced widespread fitness changes in the pool.

ence set. Hypersensitive heterozygotes resulting from the compound treatments in Group II represent the most attractive candidates for further analysis due to the relatively small number of highly significant outliers.

Fitness Profiling Identifies Known Activities of Well-Characterized Compounds

To determine the sensitivity of this method, we analyzed the results for 20 compounds with reported protein tar-

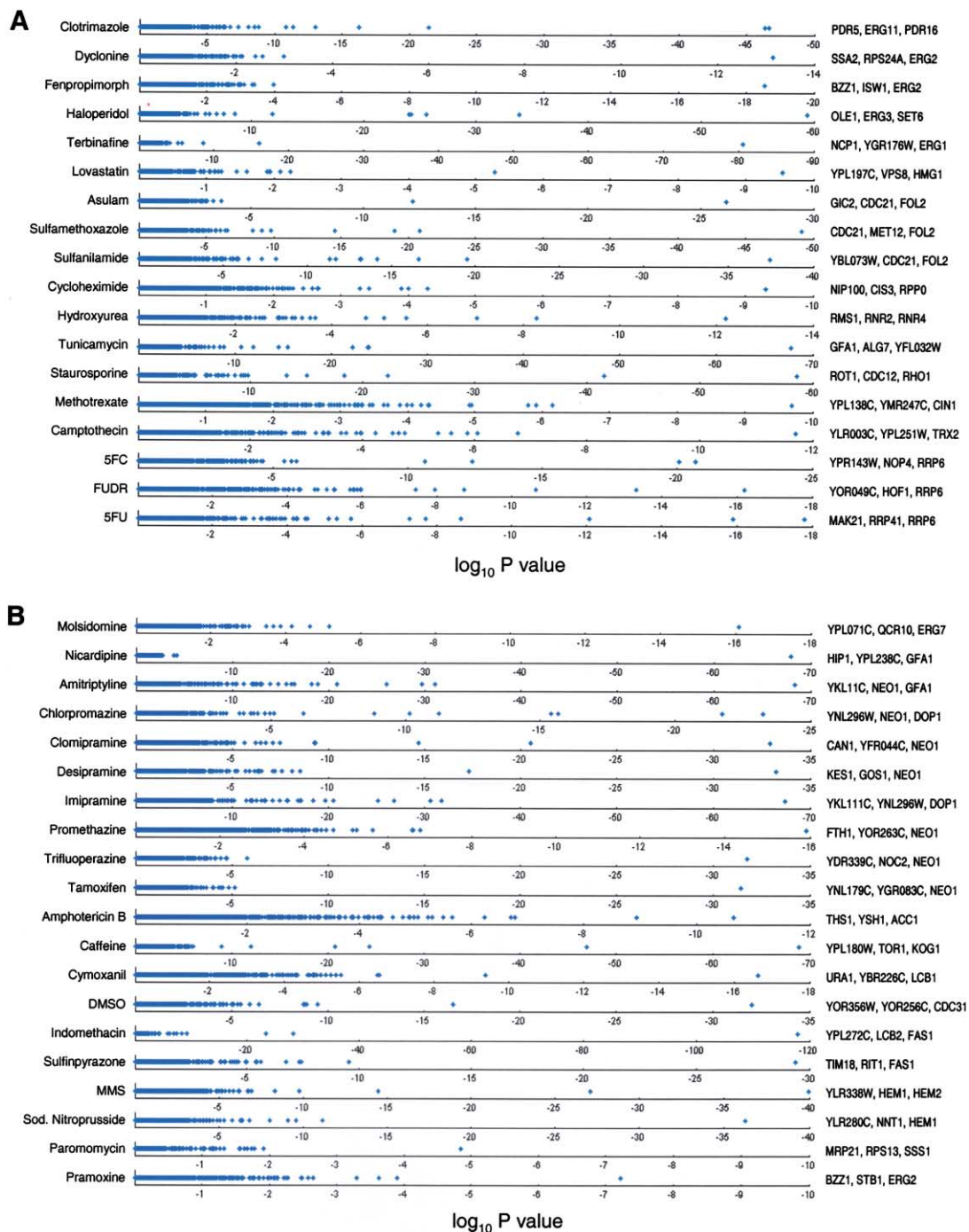


Figure 4. High Resolution View of Selected Fitness Profiles from Group II Compounds

(A) Compounds with previously reported protein targets in yeast.

(B) Selected compounds with no reported protein targets in yeast.

In Figures 4A and 4B, the three most significant outliers are listed on the right side of each P value plot and the x axis has been specifically scaled to the P value distribution of each drug treatment. Outliers are listed from left to right in order of decreasing log₁₀ P values.

gets in yeast (Table 1). The correct targets or constituents of target complexes were identified for the majority of these well-characterized compounds (Figure 4A). Six of the correctly identified targets involved compounds that inhibit distinct biochemical steps along the

ergosterol pathway. These included lovastatin (*HMG1*) (Rine et al., 1983), terbinafine (*ERG1*) (Jandrositz et al., 1991), clotrimazole (*ERG11*) (Truan et al., 1994), fenpropimorph (*ERG2*) (Marcireau et al., 1990), and dyclonine (*ERG2*) (Hughes et al., 2000). Haloperidol affected *ERG3*

and *ERG24* heterozygotes, which are adjacent to the proposed target (*ERG2*) in the pathway (Moebius et al., 1996). In addition, we found that three different sulfabased drugs (asulam, sulfamethoxazole, and sulfanilamide) affected folic acid biosynthesis as reported in the literature (Nardese et al., 1996; Patel et al., 2003). Although broad-spectrum lethality resulted from treatment with carbendazim, a benomyl-analog known to target tubulin, the most affected strains were heterozygotes of genes involved in microtubule formation (*GIM2* and *GIM3*) (Geissler et al., 1998; Neff et al., 1983). The targets were also correctly identified for compounds that inhibit the small unit of ribonucleotide reductase (hydroxyurea) (Rittberg and Wright, 1989); the 60s ribosomal subunit (cycloheximide) (Stocklein and Piepersberg, 1980); the protein kinase C complex (staurosporine) (Yoshida et al., 1992); and protein glycosylation (tunicamycin) (Barnes et al., 1984). These examples demonstrate that fitness profiling can accurately detect the cellular effects of drugs in a variety of biochemical pathways.

Some compounds with known yeast targets yielded unexpected results. Treatment with methotrexate, for example, resulted in identification of *CIN1* but not the gene (*DFR1*) encoding the known target dihydrofolate reductase (Huang et al., 1992). Given the nonessential role of Cin1p in microtubule formation, it is likely that the observed drug sensitivity resulted from a synthetic lethal interaction with the known target. In another example, camptothecin unexpectedly induced a growth defect in the *trx2/TRX2* strain, while the heterozygote of the known target gene (*TOP1*) was unaffected (Pommier et al., 1998). Identification of *TRX2*, a nonessential gene involved in the tolerance of oxidative stress, is supported by a recent report in plants showing that camptothecin induces oxidative stress via the mitochondrial respiratory chain (Weir et al., 2003). The heterozygote for *PMA1*, which encodes the H⁺-ATPase targeted by omeprazole (Monk et al., 1995), was not affected by drug treatment. This may be due to complementation of the drug-induced inhibition of Pma1p by the functionally overlapping *PMA2* protein. Finally, three compounds (5-fluorocytosine, 5-fluorouracil, and FUDR) known to inhibit Cdc21p induced growth defects in members of the rRNA processing complex in addition to the expected target (*CDC21* was one of the top 10 most affected strains) (Hardman et al., 2001). We have subsequently demonstrated that the exosome is likely to be a major cellular target for 5FU in yeast (see follow-up section on 5FU).

A number of compounds with previously unknown yeast targets induced fitness defects in specific heterozygotes (Figure 4B). Among these findings was the discovery that molsidomine blocked sterol biosynthesis at a particular step in the pathway (*ERG7*). In addition, we found that tricyclic antidepressants and tamoxifen affected *NEO1*, a P-type ATPase with a number of human homologs. Caffeine was found to inhibit the TOR protein kinase complex. Other processes such as sphingolipid synthesis, fatty acid synthesis, cell wall metabolism, and heme biosynthesis also appear to be targeted by compounds in this study. The results from treatment with 5FU and molsidomine were chosen for follow-up studies, which are described in the following sections.

Inhibition of Lanosterol Synthase (Erg7p) by Molsidomine

Molsidomine (N-ethoxycarbonyl-3-morpholino-sydnonimine) is a potent vasodilator used clinically to treat angina for the past twenty years. Enzymatic modification of molsidomine in the human liver results in derivatives (Figure 5A) that are effective nitric oxide donors, an activity that accounts for the vasodilatory properties observed in mammals (Reden, 1990). Fitness profiling revealed significant molsidomine-induced haploinsufficiency for only the *ERG7* (lanosterol synthase) heterozygote (Figure 5B). Lanosterol synthase is a highly conserved and essential component of ergosterol biosynthesis (Corey et al., 1994; Lees et al., 1995). This finding was further supported by the observation that overexpression of *ERG7* in a wild-type yeast strain confers resistance to molsidomine (Figure 5C) and that molsidomine causes an accumulation of the Erg7p substrate, 2,3-oxidosqualene (data not shown), as is observed with other Erg7p inhibitors and in an *erg7* deletion strain (Milla et al., 2002). All of these data are indicative of Erg7p inhibition.

Next, we asked whether molsidomine could block the activity of lanosterol synthase from other organisms. Specifically, we measured the effect of molsidomine and its metabolites on mammalian and bacterial homologs of *ERG7*. We found that lanosterol synthase purified from rat liver (Abe and Prestwich, 1995) was potently inhibited in vitro by SIN-1, the first metabolic derivative of molsidomine (Figure 5D). Likewise, in vitro inhibition of recombinant lanosterol synthase from *Alicyclobacillus acidocaldarius* (Ochs et al., 1992) was observed for SIN-1 (Figure 5E). Together these results indicate that molsidomine effectively blocks sterol synthesis through the inhibitory effect of its metabolite SIN-1 on lanosterol synthase. Interestingly, previous reports have shown that molsidomine lowers cholesterol levels in both rats and humans (Chassoux, 1989; Granzer and Ostrowski, 1984). As the metabolism of molsidomine in humans and rats is quite similar, providing SIN-1 as an active intermediate (Tanayama et al., 1974; Wilson et al., 1987), the results from this study identify the likely molecular mechanism for the cholesterol lowering properties of this drug.

Disruption of Exosome-Specific rRNA Processing by 5-Fluorouracil

The antiproliferative antimetabolite 5-fluorouracil (5FU) is one of the most successful and widely used chemotherapeutics for the treatment of solid tumors in cancer patients. It is thought that the major cytotoxic effects of 5FU occur at the level of DNA synthesis as a competitive inhibitor of thymidylate synthetase (Parker and Cheng, 1990). However, a growing body of evidence suggests that the antiproliferation effects of 5FU may result from inhibition of RNA metabolism (Longley et al., 2003). The most convincing argument for the role of RNA metabolism as a target of 5FU comes from experiments showing that cotreatment of cells with uridine, but not thymidine, relieves the cytotoxic and apoptotic effects of the drug (Engelbrecht et al., 1984; Linke et al., 1996; Pritchard et al., 1997).

Treatment of the heterozygous deletion pool with 5FU

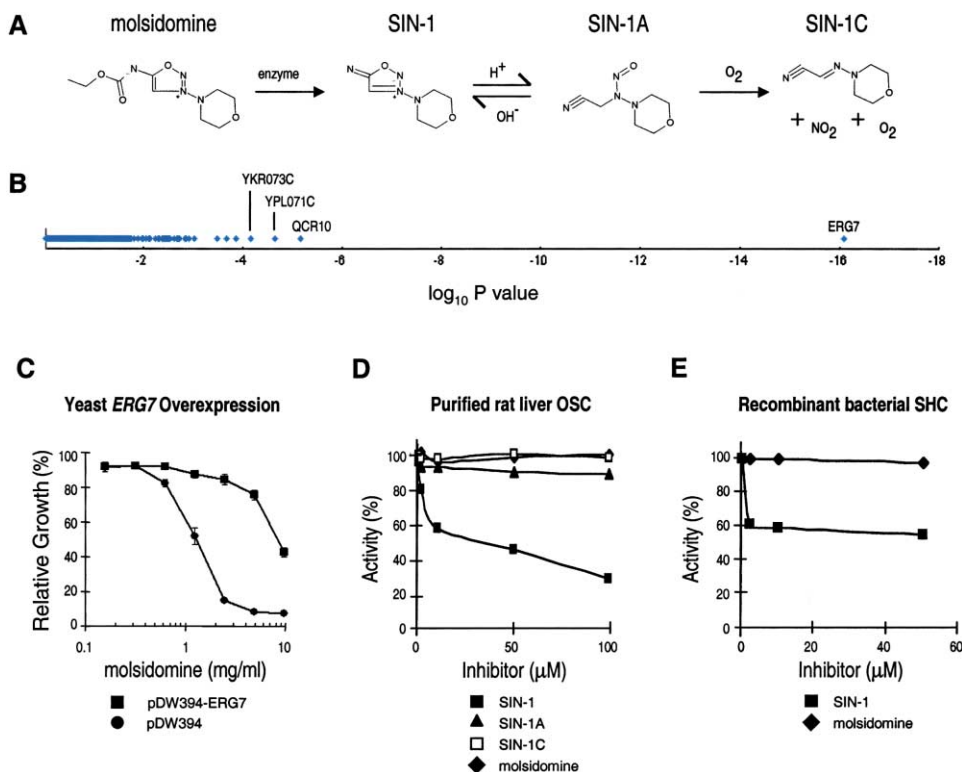


Figure 5. Inhibition of Lanosterol Synthase by Molsidomine

(A) Chemical structures and the relationships between molsidomine and its metabolites, SIN-1, SIN-1A, and SIN-1C. Molsidomine is metabolized *in vivo* by a series of transformations as illustrated. The vasodilatory properties of molsidomine occur through SIN-1C.

(B) Fitness profile of molsidomine. The top four outliers are labeled in this dot plot. The *ERG7* heterozygote displayed the most significant growth defect in response to molsidomine treatment (P value $< 1 \times 10^{-16}$).

(C) Yeast overexpression of *ERG7* confers resistance to molsidomine. A wild-type yeast strain was transformed with plasmids pDW394 (circle) or pDW394-*ERG7* (square). Overnight cultures were diluted and grown in the presence of molsidomine (0–10 mg/mL) for 15 hr. The relative growth for each strain was calculated by dividing the optical density of the drug-treated culture by that of the untreated control. Each condition was carried out in triplicate.

(D) Inhibition of purified rat liver oxidosqualene cyclase (OSC) activity. The *in vitro* conversion of [¹⁴C] 2,3-oxidosqualene by purified OSC was measured after incubation at 37°C for 30 min with purified OSC. The conversions were analyzed by radio-TLC. The percent activity was calculated by dividing each value from the drug treatment by that of the untreated control.

(E) Inhibition of recombinant bacterial squalene:hopene cyclase (SHC) activity. The *in vitro* conversion of [¹⁴C]-squalene by recombinant SHC was measured after incubation at 30°C for 30 min. The conversions were analyzed by radio-TLC. The percent activity was calculated by dividing each value from the drug treatment by that of the untreated control.

revealed drug-induced haploinsufficiency for eight genes that play roles in ribosome biogenesis in addition to the previously reported target *CDC21* (Figure 6A). Four of the seven genes (*RRP6*, *RRP41*, *RRP44*, and *RRP46*) encode components of the exosome, a conserved complex required for 5.8S rRNA and snoRNA 3' end processing (Butler, 2002; Mitchell and Tollervey, 2000). The other four genes, *NOP4*, *MAK21*, *SSF1*, and *YPR143W*, play roles in either 25S rRNA processing, 60S ribosome production, 27S rRNA processing, or associate with other nucleolar components (Edskes et al., 1998; Fatica et al., 2002; Ho et al., 2002; Sun and Woolford, 1994).

To further characterize the effect of 5FU, we monitored rRNA intermediates in normal and mutant yeast strains following drug treatment. Figure 6B outlines the major events in rRNA processing, which begins with synthesis of the 35S pre-rRNA by RNA polymerase I and proceeds by a series of endo- and exonucleolytic cleavages that yield three of the four mature rRNAs

(Venema and Tollervey, 1999). We monitored the removal of internal transcribed spacers, ITS1 and ITS2, by Northern blot analysis using ITS-specific oligonucleotide probes (Figure 6C). We found that 5FU treatment causes the accumulation of an rRNA processing product we refer to as A2-C2 (Figure 6C). In addition, 5FU treatment causes a transient increase in 35S pre-rRNA levels similar to the effects of depletion of individual exosome components, including Rrp6p, Rrp41p, and Rrp44p (Allmang et al., 2000). Interestingly, the untreated *rrp6Δ* strain displays a phenocopy of the 5FU-induced accumulation of the A2-C2 rRNA processing product (Figure 6C).

Next, we asked whether 5FU treatment enhanced the accumulation of A2-C2 in specific heterozygous deletion strains identified in this study. The wild-type control and each of the heterozygotes were grown in the presence of 5FU followed by Northern blot analysis to measure A2-C2 levels (Figure 6D). Strains that were heterozygous for components of the exosome (*RRP6*, *RRP41*, *RRP44*,

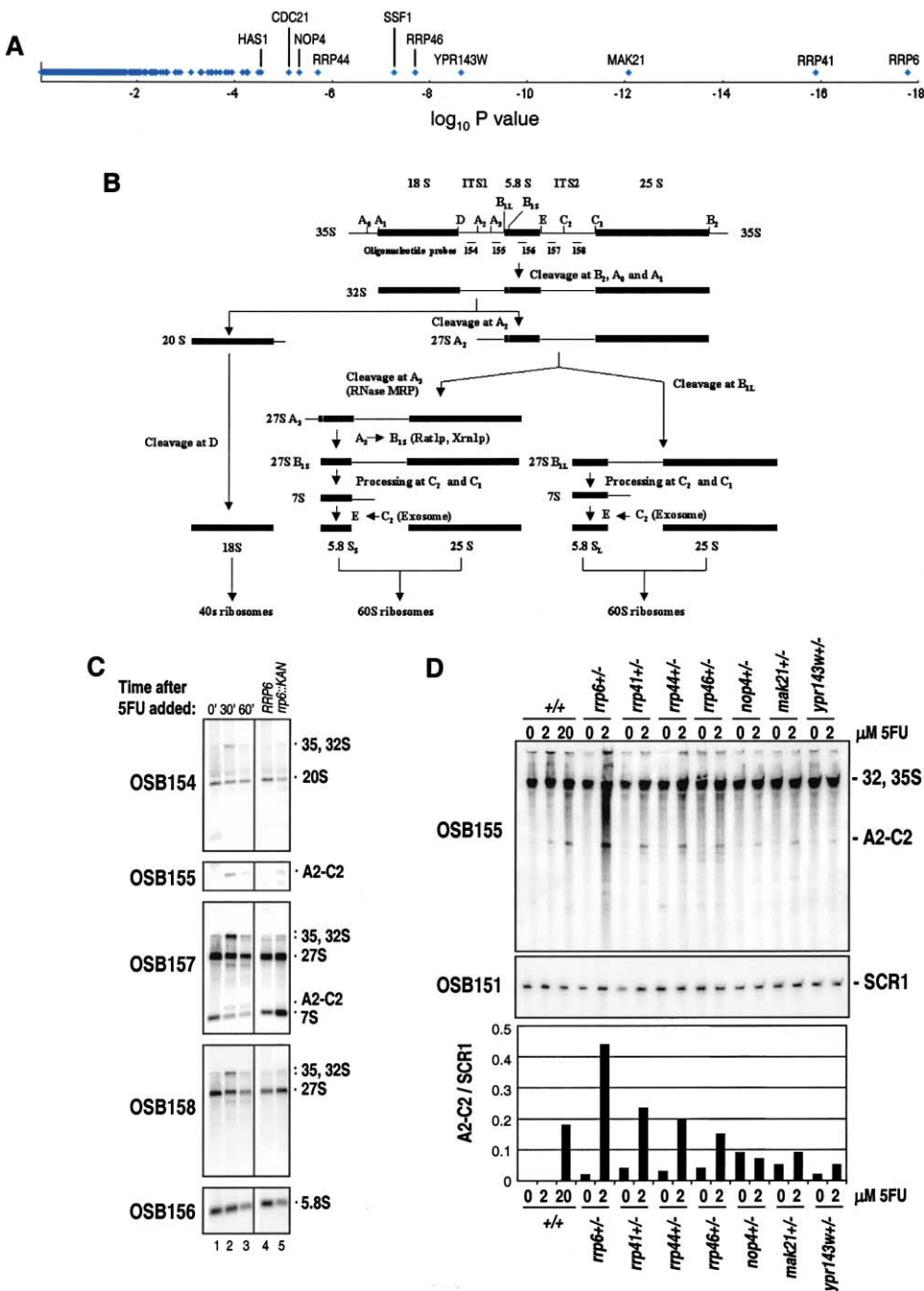


Figure 6. Disruption of Exosome Specific rRNA Processing by 5FU

(A) Fitness Profile of 5FU. Eight of the top ten outliers (*RRP6*, *RRP41*, *MAK21*, *YPR143W*, *RRP46*, *SSF1*, *RRP44*, *NOP4*) play roles in ribosome biogenesis. *CDC21*, the reported target of 5FU, is also among the top ten outliers.

(B) Diagram of the major events of rRNA processing in *S. cerevisiae*. The positions complementary to oligonucleotide probes used are indicated below the 35S pre-rRNA. Processing begins with cleavage of the 35S precursor rRNA (35S pre-rRNA) at sites A_0 and A_1 in the 5' external transcribed spacer (5' ETS) and at B_2 to yield the 32S pre-rRNA. Next, cleavage of 32S pre-rRNA yields 27S pre-rRNA and 20S pre-rRNA, which is converted to mature 18S rRNA by further cleavage. The 27S pre-rRNA follows either of two parallel pathways each of which yields mature 25S rRNA. The pathways differ in the mechanism that generates the mature 5' end of 5.8S rRNA. The exosome and Rrp6p form the 3' end of 5.8S rRNA by exonucleolytic removal of the 3' end of 7S pre-rRNA: the exosome removes all but the last 30 nucleotides, which is then trimmed off by Rrp6p.

(C) Northern blot analysis of rRNA processing intermediates. A wild-type diploid was treated in culture with 200 μ M 5FU and RNA was prepared from samples taken at the times indicated at the top of the figure (lanes 1–3). RNA was also prepared from an untreated wild-type haploid (lane 4) and an isogenic *rrp6::KAN* mutant (lane 5). The blot was probed with radiolabeled oligonucleotides (indicated at the left of each image) complementary to specific pre-rRNA intermediates and mature 5.8S rRNA. Notation to the right of each image indicates the identity of the major pre-rRNA intermediates.

and *RRP46*) produced 2- to 10-fold more A2-C2 than the wild-type strain treated with 5FU (Figure 6D). Although there is evidence that 5FU may result in general RNA damage, our results reveal a specific molecular mechanism by which 5FU may inhibit cell growth through perturbation of rRNA processing by the exosome complex. In fact, preliminary data suggest that 5FU prolongs the time yeast cells spend in G2/M and that this effect is exacerbated by the exosome mutations (data not shown).

Discussion

Use of Fitness Profiling For Understanding Drug Activities

We have demonstrated that fitness profiling is a powerful approach for analyzing the modes of action of clinically relevant compounds. Identifying the protein targets of existing drugs can reveal sources of pharmacologically desirable side effects in addition to the mechanisms for unwanted toxicities. Understanding the molecular mechanisms for therapeutic compounds is also critical because it allows researchers to develop second-generation compounds with improved pharmacological properties. Knowing the cellular targets for clinically proven small molecules can also reveal drug targets that are already validated in humans.

This highly parallel and sensitive yeast assay offers several key advantages over traditional approaches for analyzing drug activities. First, this approach requires no prior knowledge of compound mode of action, which allows truly novel drug activities to be uncovered in a systematic and unbiased fashion. For example, we found that the tricyclic antidepressants (amitriptyline, imipramine, desipramine, clomipramine, chlorpromazine, and trifluoperazine) affected the growth of the *NEO1* heterozygote (Figure 3C). *NEO1* encodes an integral membrane protein in the P-type ATPase superfamily (Axelsen and Palmgren, 1998). Although the primary mode of antidepressive action of these compounds occurs by the nonselective inhibition of neurotransmitter reuptake, these compounds confer a number of deleterious side effects by mechanisms that are poorly understood (Hardman et al., 2001). Evidence for TCA inhibition of ATPase activity has been documented in human erythrocyte plasma membranes and skeletal sarcoplasmic reticulum membranes (Plenge-Tellechea et al., 1999; Soler et al., 2000). We found that the growth rate of the *NEO1* heterozygote was also impeded by tamoxifen, a potent antiestrogen drug for the treatment of breast cancer. The chemical structures of the tricyclics and tamoxifen interestingly share a common lipophilic moiety characterized by an amine tail. Additional studies will be needed to further characterize the putative effects of these compounds on ATPase activity in yeast and humans.

Another advantage of the fitness assay is that biological processes that are affected by a given compound are identified in addition to the precise protein target(s). For example, treatment of the heterozygous deletion pool with 5FU resulted in the identification of a group of genes that encode components of the exosome complex. Another example involved the drug tunicamycin, which is known to affect protein glycosylation. Besides identifying the known target (*ALG7p*), heterozygotes involved in either the endoplasmic reticulum (ER) stress response (*HAC1*) or cell wall glycosylation (*GFA1*) also displayed sensitivity to tunicamycin. Finally, identification of the *fol2/FOL2* strain in response to the sulfabased drugs or the *cdc21/CDC21* and *rho1/RHO1* strains following staurosporine treatment also confirms the effectiveness of this assay in detecting affected pathways.

The dataset presented here has yet to be fully mined and offers opportunities for many follow-up experiments. Of the 56 compounds yielding clear outliers, we chose two examples for in-depth characterization by conventional experimental techniques. In the first example, fitness results suggesting that lanosterol synthase (*Erg7p*) may be a target of molsidomine were confirmed in yeast by overexpression resistance and biochemical analyses of pathway intermediates. This work was further validated by monitoring the inhibitory activity of this compound on the bacterial and mammalian enzymes *in vitro*. Interestingly, the cholesterol-lowering effect of molsidomine appears to be distinct from the nitric oxide releasing activity, which accounts for the drug's vasodilatory properties. This new information provides potential clinical validation for lanosterol synthase as a safe and effective target for the development of new cholesterol-lowering drugs.

In the second example, we performed a set of experiments to confirm the hypothesis that 5FU blocks rRNA processing by the exosome, which may account for some of this drug's antiproliferation activities. At present it remains unclear how inhibition of the exosome by 5FU inhibits cellular growth. Defects in rRNA processing could potentially cause inhibition of protein synthesis. Alternatively, recent evidence suggests that tumor suppressor proteins such as nucleolar ARF may mediate crosstalk between the rRNA processing pathway and components that regulate cell cycle progression (Itahana et al., 2003; Ruggero and Pandolfi, 2003). Our preliminary data (not shown) also suggest that 5FU affects cell cycle timing in yeast that is exacerbated by mutations in exosome components. Hence, these findings are significant in light of a growing body of research indicating a critical relationship between ribosome biogenesis and cell cycle control (Du and Stillman, 2002; Ruggero et al., 2003; Sugimoto et al., 2003; Volarevic et al., 2000). Moreover, the cytotoxic effects of 5FU in human cells may result from p53-mediated effects on RNA

(D) Analysis of A2-C2 rRNA processing product accumulation in wild-type ($^{+/+}$) and mutant yeast strains treated for 30 min with the indicated concentration of 5FU. The top image is a Northern blot probed with OSB155 (see Figure 6B) and the central image shows the same blot probed with an oligonucleotide complementary to SCR1 RNA (OSB151). The graph illustrates the level of A2-C2 rRNA processing product determined by storage phosphorimager analysis and normalized to the level of SCR1 for each strain and is the average of two independent experiments.

metabolism. This is supported by data showing that administration of the drug causes apoptosis in p53^{+/+}, but not in p53^{-/-} intestinal epithelial cells. In addition, coadministration of 5FU with uridine, but not thymidine, inhibited 5FU-induced apoptosis (Pritchard et al., 1997). The dependence of 5FU action on p53 and connections between p53 and rRNA metabolism suggest that the p53 pathway may act as a sensor of defects in rRNA processing thereby signaling cell cycle arrest and/or apoptosis. A clear understanding of the role of the exosome in the p53 response to 5FU may provide a new opportunity for therapeutic intervention in the treatment of cancer.

Limitations and Technical Considerations

While the fitness assay is a powerful approach for identifying drug targets, there are also a number of limitations. First, the compound of interest must be able to affect the growth rate of the cell. Failure of a compound to impart a fitness defect may indicate that (1) the drug target is not encoded in the yeast genome; (2) drug effects are masked by other proteins with redundant activities; (3) the drug was not correctly metabolized; or (4) the drug was not able to enter the cell. However, the ability of a compound to affect the growth rate of yeast does not guarantee that a target will be identified by this approach. In order for this approach to work, a heterozygote for the target gene must be present in the mutant pool. Unfortunately, heterozygotes representing only about half of the yeast genome were available at the time of this study, which resulted in a lower detection rate than would be expected from a full genome pool. Failure to detect the precise protein targets of staurosporine (*PKC1*) and the sulfa-based drugs (*FOL1* and *FOL3*) can be attributed to the fact that the target strains were not in the pool. Another requirement of this assay is that the activity level of the targeted protein must be influenced by the dosage level of the corresponding gene under the conditions profiled. Finally, compounds that exert their effects through direct interaction with nonprotein elements in the cell, such as DNA (actinomycin D) or ergosterol (amphotericin B), do not appear suitable for this approach.

In some cases, the increased drug sensitivities of heterozygotes are caused by indirect effects on the cell and do not represent primary drug targets. For instance, members of the multidrug resistant (MDR) family of transporters (e.g., *PDR5*) were implicated in a number of drug treatments. These nonessential efflux pumps act to reduce the effective intracellular concentration of certain structural classes of compounds. Deletion of one of the two copies of these genes in a diploid cell can result in a reduced capacity to export drugs from the cell, thereby causing a hypersensitivity phenotype of the heterozygotes. Comparison of gene expression profiles from putative target deletion strains with those of drug treatments can help distinguish actual drug targets from proteins involved in an indirect cellular drug response (Hughes et al., 2000).

Some of the candidate targets identified with this approach are due to artifacts that were introduced during the construction of the deletion strains. For example, the heterozygote for *YML176C* displayed increased sensitivity to terbinafine (P value = 1×10^{-16}) indicating

that this gene encodes a potential target for this drug. However, the open reading frame of *YML176C* overlaps with *ERG1* (*YML175C*), the known target of terbinafine, which suggests that the sensitivity of this heterozygote was likely due to the inadvertent disruption of the *ERG1* open reading frame. Similarly, background mutations that are unlinked to the heterozygous locus or crosshybridizing tags may also result in false positives. The number of false positives can be minimized by confirming the fitness results with the individual deletion strains and testing whether overexpression of the candidate gene confers resistance to the drug of interest.

A critical component of this study was the use of a strain-specific error model to identify drug-dependent effects that are statistically significant. Since some heterozygotes have nonspecific growth defects, it is necessary to understand the normal behavior of each strain before calculating drug-induced effects. We determined that a reference set must be populated with a minimum of 50 experiments and that chemical treatments are more effective compared to nontreated controls for the reference set. When performed as described here, this method will detect as little as 5–10% growth deficits in individual strains (data not shown). However, it is important to note that each study must generate its own reference set due to the inherent variability of experimental conditions. Sensitivity could theoretically be increased by extending the pool outgrowth beyond 20 generations and by increasing the number of experiments included in the reference set. We have also found that P values from this approach provide an effective way to rank order the strains in a given drug treatment to identify the significant outliers. The ability to compare P values across compounds is limited by the fact that compounds have very diverse modes of action and the doses of different compounds cannot be considered equivalent.

Future Directions

We have demonstrated that fitness profiling is a powerful approach for studying the activities of clinically relevant compounds in yeast. Tagged heterozygous deletion strains have been made available for virtually every gene in the yeast genome since this study was completed. This resource coupled with commercially available tag arrays make it possible to extend this type of analysis to the full genome level. In addition, a similar strategy using pools of homozygous deletion strains could be used to reveal targets that are currently masked by redundant activities. Growth conditions can also be modified to assess drug sensitivities of genes that are expressed only under certain physiological conditions. Recently developed techniques to introduce specific mutations into all strains of a deletion pool make it possible to identify drug effects in a variety of different genetic backgrounds (Ooi et al., 2001). Finally, fitness profiling results can be combined with data from other large-scale functional genomics efforts to enhance our understanding of compound activities.

Experimental Procedures

Supplemental Data

A comprehensive list of P values for all experiments discussed here is available on the *Cell* website. Log ratio data is available upon request.

Yeast Strains and Plasmids

Isoogenic heterozygous deletion strains were obtained from the *Saccharomyces* Genome Deletion Consortium (Winzeler et al., 1999). A plasmid expressing yeast *ERG7* was constructed by PCR amplification of the open reading frame from yeast genomic DNA. The ORF was cloned by in vivo recombination into pDW394, a high copy URA3 vector with expression driven by the *HOR7* promoter.

Construction of Heterozygous Deletion Pool

The collection of 3503 heterozygous deletion strains was obtained from the *Saccharomyces* Deletion Consortium (see website for strain and tag information: http://www-sequence.stanford.edu/group/yeast_deletion_project/Enter_function.html) as saturated glycerol stocks in 96-well plates. Strains were transferred to YEPD agar plates with a 96-well colony replicator (V & P Scientific, Inc., San Diego, CA) and were grown at 30°C for 72 hr. All colony-forming units were collected with a rubber spatula and combined in a 50 ml conical tube. The cell mixture was washed in 30 ml of YEPD and diluted to 1×10^{10} cells per mL in YEPD with 15% glycerol. Single use 2 ml aliquots were flash-frozen in a dry ice/ethanol bath and stored at -80°C until use.

Drug Treatments

To determine the appropriate drug treatment concentrations, a 5-fold dilution series of each compound was made in synthetic complete medium with 2% glucose and 2% (w/v) casamino acids (SCC) for eleven 2× drug concentrations and one vehicle control. A 100 μl aliquot of each dose was distributed to a 96-well tissue culture plate in triplicate. Subsequently, a 2× cell suspension was made by thawing an aliquot of the frozen deletion pool on ice before harvesting by centrifugation, washing twice with SCC, and diluting to 2.65×10^4 cells/ml in SCC at room temperature. A 100 μl aliquot of the 2× cell mixture was then added to each of the 96 wells in the drug-containing tissue culture plate. Plates were then incubated at 30°C with gentle agitation on a rotary shaker for 15 hr reaching a density of 1.3×10^7 cells per mL (vehicle control). The pool fitness (PF) was calculated ($PF = 1 + [(\log(OD_{600, \text{treated}}) / OD_{600, \text{untreated}})] / (\log(2)^g)$), where g is the number of generations assumed to be 10) for each drug concentration and doses that resulted in $0.70 \leq PF \leq 0.96$ were selected for fitness profiling experiments.

Fitness Profiling

An aliquot of the frozen pool was thawed at room temperature and diluted in 100 ml of SCC to a final density of 1.3×10^7 cells/ml. A 5 ml aliquot was harvested immediately (G-0) by centrifugation and frozen at -80°C until DNA isolation. Dilutions of 1.3×10^4 cells/ml in 20 ml aliquots were grown at 30°C for 10 generations to a density of 1.3×10^7 cells/ml. Cultures were then diluted once again to 1.3×10^4 cells/ml in fresh media or fresh media containing drug. After another ten population doublings, 1×10^8 cells from each culture were harvested (G-20) as described above. All harvested cell pellets were thawed on ice and subjected to a 30 s, 50 krpm mechanical lysis with 0.5 mm glass beads in a Mini-Beadbeater (Biospec Products, Bartlesville, OK). Genomic DNA was subsequently isolated using the MasterPure Yeast DNA Purification Kit (Epicentre #mpy80200), quantified, and normalized to 15 ng/μl.

Tag Amplification and Hybridization to DNA Microarrays

For each treatment, genomic DNA isolated from cultures harvested at G-0 and G-20 culture was labeled with Cy3 and Cy5, respectively. The UP tag and DOWN tag barcodes were amplified and labeled in separate 50 μl reactions with 1 μl (15 ng) of genomic DNA, 5 μl of UP tag or DOWN tag primer mix, and 44 μl of PCR SuperMix (PCR Platinum SuperMix, Gibco #11306-016). The UP tag primer mix contained 5 μM of unlabeled UP tag forward primer (5'-gagtgccac gaggctct-3' and Cy3- or Cy5-labeled reverse UP tag primer (5'-Cy-gtcgacctgcagcgtacg-3'). The DOWN tag primer mix contained 5 μM of Cy3- or Cy5-labeled DOWN tag forward primer (5'-Cy-cgagctc gaattcatcg-3') and 5 μM of unlabeled DOWN tag reverse primer (5'-cgggtgtcggctctcgtag-3'). PCR conditions were as follows: 5 min at 94°C; then 35 cycles of 30 s at 94°C; 30 s at 50°C; and 30 s at 72°C followed by 7 min at 72°C to ensure product elongation. Blocking primers complementary to the common priming sites were annealed prior to hybridization. Labeled tags were hybridized to DNA microar-

rays consisting of either 5873 UP tag probes or 5873 DOWN tag probes. DNA microarrays consisting of 20-mer probes (see strain information for probe sequences) were synthesized as described in Hughes et al. (2000). Hybridizations were done in 3.5 ml of 1× SSTE hybridization buffer (1 M NaCl, 10 mM Tris [pH 7.0], 0.5% Triton X-100) containing 10 pM gridline DNA for 3 hr at 40°C. Arrays were first washed in 6× SSPE + 0.05% Triton-X and then in ice-cold 0.06× SSPE. Slides were then scanned on a GMS 418 scanner (Genetic Microsystems, Woburn, MA).

Data Analysis

Descriptions of formulas used for array quantitation and P value derivation are available on the *Cell* website.

Northern Blot Analysis

rRNA processing was analyzed by Northern blot analysis of total RNA samples as described by Briggs et al. (1998). Transfer membranes were hybridized with 5' ³²P-labeled deoxyribonucleotides OSB151 (5'-gtctagccgcgaggaagg-3'); OSB155 (5'-tccagttacgaaaat tctgttttgacaa-3'); OSB154 (5'-tctgtcccagtaaaagctctcatcg-3'); OSB158 (5'-gttcgcctagacgctctcttc-3'); OSB157 (5'-gggtgaccaatt caagta-3'); OSB156 (5'-cgctgcttctcatcgatcg-3'); or OSB138 (5'-tcagagatcttggtgataa-3'), which are complementary to SCR1 RNA, ITS1, ITS2, and 5.8S, respectively (Figure 6B). Blots were analyzed by storage phosphorimager analysis.

Enzyme Activity Assay

Chemicals

(3S)-[24,30]2,3-oxidosqualene was synthesized as described by Bai et al. (1998). Triton X-100 was purchased from Sigma. Molsidomine, SIN-1-hydrochloride, and SIN-1A/γCD complex (10%, w/w SIN-1A content) were obtained from Alexis Biochemicals.

Biological Materials

Rat liver lanosterol cyclase was purified according to the procedure described by Abe and Prestwich (1995).

Enzyme Assay for OSC

The reaction mixture contained 100 mM sodium citrate, [pH 7.4], 0.1% (v/v) Triton X-100, 5 μM [¹⁴C]2,3-oxidosqualene (52.6 mCi/mmol), and 5 μg of purified enzyme in a final volume of 1 mL. After incubation at 37°C for 30 min, the reaction was stopped by addition of 1 ml CH₂Cl₂. The extract was concentrated using a Speed-Vac, and then subjected to silica gel TLC (Whatmann LK6D). The TLC plates were developed with CH₂Cl₂. The conversions were then analyzed by radio-TLC (Bio-Scan, System 200 Imaging Scanner). All assays were carried out in triplicate.

Enzyme Assay for SHC Bacterial Lanosterol Cyclase

Recombinant *A. acidocaldarius* lanosterol cyclase was expressed in *E. coli* and purified as outlined by Ochs et al (1992). To 50 μl of 5 mM sodium citrate, [pH 6.0], 0.1% (v/v) Triton X-100 was added 4 μl of a solution of SHC (600 μg/ml) and 3 μl (0.021 μCi) of [¹⁴C]-squalene (1 mM in ethanol, 7 mCi/mmmole). After incubation at 60°C for 30 min, the reaction was stopped by addition of 1 ml CH₂Cl₂. The extract was concentrated using a Speed-Vac and then subjected to silica gel TLC. The TLC plates were developed to a distance of 5 cm in chloroform and after drying for 15 cm in hexane. The conversions were then analyzed by radio-TLC.

Acknowledgments

We thank H. Dai, R. Stoughton, A. Adams, A. Sachs, and S. Friend for many helpful discussions; M. Kuo for literature research on compounds profiled in this study; J. Koch, T. Ward, J. Burchard, and E. Coffey for technical assistance; and C. Raymond and L. Lim for comments on the manuscript. We are grateful to all members of the *Saccharomyces* Deletion Consortium for their efforts. We apologize to the many researchers whose work could not be cited due to space considerations and refer the reader to the *Saccharomyces* Genome Database (<http://www.yeastgenome.org>) for information and references for specific gene products. This work was supported by Rosetta Inpharmatics, LLC; two grants from the Public Health Service (GM59898 and CA95913) to J.S.B.; a grant from the National Institutes of Health (GM62104) to M.B.; and a grant (GM 44836) to G.D.P.

Received: October 30, 2003
Revised: November 24, 2003
Accepted: December 16, 2003
Published online: December 24, 2003

References

- Abe, I., and Prestwich, G.D. (1995). Molecular cloning, characterization, and functional expression of rat oxidosqualene cyclase cDNA. *Proc. Natl. Acad. Sci. USA* **95**, 9274–9278.
- Allmang, C., Mitchell, P., Petfalski, E., and Tollervey, D. (2000). Degradation of ribosomal RNA precursors by the exosome. *Nucleic Acids Res.* **28**, 1684–1691.
- Axelsen, K.B., and Palmgren, M.G. (1998). Evolution of substrate specificities in the P-type ATPase superfamily. *J. Mol. Evol.* **46**, 84–101.
- Bai, M., Xiao, X.Y., and Prestwich, G.D. (1998). Epoxidation of 2,3 oxidosqualene to 2,3;22,23-squalene dioxide by squalene epoxidase. *Biochem. Biophys. Res. Commun.* **185**, 323–329.
- Barnes, G., Hansen, W.J., Holcomb, C.L., and Rine, J. (1984). Asparagine-linked glycosylation in *Saccharomyces cerevisiae*: genetic analysis of an early step. *Mol. Cell. Biol.* **4**, 2381–2388.
- Briggs, M.W., Burkard, K.T., and Butler, J.S. (1998). Rrp6p, the yeast homologue of the human PM-Sc1 100-kDa autoantigen, is essential for efficient 5.8 rRNA 3' end formation. *J. Biol. Chem.* **273**, 13255–13263.
- Butler, J.S. (2002). The yin and yang of the exosome. *Trends Cell Biol.* **12**, 90–96.
- Chassoux, G. (1989). Molsidomine and lipid metabolism. *J. Cardiovasc. Pharmacol.* **14** (Suppl 11), S137–S138.
- Corey, E.J., Matsuda, S.P., and Bartel, B. (1994). Molecular cloning, characterization, and overexpression of ERG7, the *Saccharomyces cerevisiae* gene encoding lanosterol synthase. *Proc. Natl. Acad. Sci. USA* **91**, 2211–2215.
- Du, Y.C., and Stillman, B. (2002). Yph1p, an ORC-interacting protein: potential links between cell proliferation control, DNA replication, and ribosome biogenesis. *Cell* **109**, 835–848.
- Edskes, H.K., Ohtake, Y., and Wickner, R.B. (1998). Mak21p of *Saccharomyces cerevisiae*, a homolog of human CAATT-binding protein, is essential for 60 S ribosomal subunit biogenesis. *J. Biol. Chem.* **273**, 28912–28920.
- Engelbrecht, C., Ljungquist, I., Lewan, L., and Yngner, T. (1984). Modulation of 5-fluorouracil metabolism by thymidine. In vivo and in vitro studies on RNA-directed effects in rat liver and hepatoma. *Biochem. Pharmacol.* **33**, 745–750.
- Fatica, A., Cronshaw, A.D., Dlakic, M., and Tollervey, D. (2002). Ssf1p prevents premature processing of an early pre-60S ribosomal particle. *Mol. Cell* **9**, 341–351.
- Foury, F. (1997). Human genetic diseases: a cross-talk between man and yeast. *Gene* **195**, 1–10.
- Geissler, S., Siegers, K., and Schiebel, E. (1998). A novel protein complex promoting formation of functional alpha- and gamma-tubulin. *EMBO J.* **17**, 952–966.
- Giaever, G., Shoemaker, D.D., Jones, T.W., Liang, H., Winzeler, E.A., Astromoff, A., and Davis, R.W. (1999). Genomic profiling of drug sensitivities via induced haploinsufficiency. *Nat. Genet.* **21**, 278–283.
- Granzer, E., and Ostrowski, J. (1984). Lipoprotein regulatory effect of molsidomine in rats. *Arzneimittelforschung* **34**, 191–193.
- Hardman, J.G., Limbard, L.E., and Goodman Gilman, A. (2001). *Goodman and Gilman's The Pharmacological Basis of Therapeutics*, 10th ed. (New York, NY: McGraw-Hill).
- Heitman, J., Movva, N.R., and Hall, M.N. (1991). Targets for cell cycle arrest by the immunosuppressant rapamycin in yeast. *Science* **253**, 905–909.
- Ho, Y., Gruhler, A., Heilbut, A., Bader, G.D., Moore, L., Adams, S.L., Millar, A., Taylor, P., Bennett, K., Boutlier, K., et al. (2002). Systematic identification of protein complexes in *Saccharomyces cerevisiae* by mass spectrometry. *Nature* **415**, 180–183.
- Huang, T., Barclay, B.J., Kalman, T.I., von Borstel, R.C., and Hastings, P.J. (1992). The phenotype of a dihydrofolate reductase mutant of *Saccharomyces cerevisiae*. *Gene* **121**, 167–171.
- Huels, C., Muellner, S., Meyer, H.E., and Cahill, D.J. (2002). The impact of protein biochips and microarrays on the drug development process. *Drug Discov. Today* **7**, S119–S124.
- Hughes, T.R., Marton, M.J., Jones, A.R., Roberts, C.J., Stoughton, R., Armour, C.D., Bennett, H.A., Coffey, E., Dai, H., He, Y.D., et al. (2000). Functional discovery via a compendium of expression profiles. *Cell* **102**, 109–126.
- Itahana, K., Bhat, K.P., Jin, A., Itahana, Y., Hawke, D., Kobayashi, R., and Zhang, Y. (2003). Tumor suppressor ARF degrades B23, a nucleolar protein involved in ribosome biogenesis and cell proliferation. *Mol. Cell* **12**, 1151–1164.
- Jandrositz, A., Turnowsky, F., and Hogenauer, G. (1991). The gene encoding squalene epoxidase from *Saccharomyces cerevisiae*: cloning and characterization. *Gene* **107**, 155–160.
- Knopp, R.H. (1999). Drug treatment of lipid disorders. *N. Engl. J. Med.* **341**, 498–511.
- Lander, E.S., Linton, L.M., Birren, B., Nusbaum, C., Zody, M.C., Baldwin, J., Devon, K., Dewar, K., Doyle, M., FitzHugh, W., et al. (2001). Initial sequencing and analysis of the human genome. *Nature* **409**, 860–921.
- Lees, N.D., Skaggs, B., Kirsch, D.R., and Bard, M. (1995). Cloning of the late genes in the ergosterol biosynthetic pathway of *Saccharomyces cerevisiae*—a review. *Lipids* **30**, 221–226.
- Linke, S.P., Clarkin, K.C., Di Leonardo, A., Tsou, A., and Wahl, G.M. (1996). A reversible, p53-dependent G0/G1 cell cycle arrest induced by ribonucleotide depletion in the absence of detectable DNA damage. *Genes Dev.* **10**, 934–947.
- Longley, D.B., Harkin, D.P., and Johnston, P.G. (2003). 5-fluorouracil: mechanisms of action and clinical strategies. *Nat. Rev. Cancer* **3**, 330–338.
- MacBeath, G., and Schreiber, S.L. (2000). Printing proteins as microarrays for high-throughput function determination. *Science* **289**, 1760–1763.
- Marcireau, C., Guilloton, M., and Karst, F. (1990). In vivo effects of fenpropimorph on the yeast *Saccharomyces cerevisiae* and determination of the molecular basis of the antifungal property. *Antimicrob. Agents Chemother.* **34**, 989–993.
- Millá, P., Athenstaedt, K., Viola, F., Oliaro-Bosso, S., Kohlwein, S.D., Daum, G., and Balliano, G. (2002). Yeast oxidosqualene cyclase (Erg7p) is a major component of lipid particles. *J. Biol. Chem.* **277**, 2406–2412.
- Mitchell, P., and Tollervey, D. (2000). Musing on the structural organization of the exosome complex. *Nat. Struct. Biol.* **7**, 843–846.
- Moebius, F.F., Bermoser, K., Reiter, R.J., Hanner, M., and Glossmann, H. (1996). Yeast sterol C8–C7 isomerase: identification and characterization of a high-affinity binding site for enzyme inhibitors. *Biochemistry* **35**, 16871–16878.
- Monk, B.C., Mason, A.B., Abramochkin, G., Haber, J.E., Seto-Young, D., and Perlin, D.S. (1995). The yeast plasma membrane proton pumping ATPase is a viable antifungal target. I. Effects of the cysteine-modifying reagent omeprazole. *Biochim. Biophys. Acta* **1239**, 81–90.
- Nardese, V., Gutlich, M., Brambilla, A., and Carbone, M.L. (1996). Disruption of the GTP-cyclohydrolase I gene in *Saccharomyces cerevisiae*. *Biochem. Biophys. Res. Commun.* **218**, 273–279.
- Neff, N.F., Thomas, J.H., Grisafi, P., and Botstein, D. (1983). Isolation of the beta-tubulin gene from yeast and demonstration of its essential function in vivo. *Cell* **33**, 211–219.
- Ochs, D., Kaletta, C., Entian, K.D., Beck-Sickinger, A., and Poralla, K. (1992). Cloning, expression, and sequencing of squalene-hopene cyclase, a key enzyme in triterpenoid metabolism. *J. Bacteriol.* **174**, 298–302.
- Ooi, S.L., Shoemaker, D.D., and Boeke, J.D. (2001). A DNA microarray-based genetic screen for nonhomologous end-joining mutants in *Saccharomyces cerevisiae*. *Science* **35**, 2552–2556.
- Parker, W.B., and Cheng, Y.C. (1990). Metabolism and mechanism of action of 5-fluorouracil. *Pharmacol. Ther.* **48**, 381–395.

- Patel, O., Satchell, J., Baell, J., Fernley, R., Coloe, P., and Macreadie, I. (2003). Inhibition studies of sulfonamide-containing folate analogs in yeast. *Microb. Drug Resist.* **9**, 139–146.
- Phizicky, E., Bastiaens, P.I., Zhu, H., Snyder, M., and Fields, S. (2003). Protein analysis on a proteomic scale. *Nature* **422**, 208–215.
- Plenge-Tellechea, F., Soler, F., and Fernandez-Belda, F. (1999). Tricyclic antidepressants inhibit the Ca²⁺-dependent ATPase activity from plasma membrane. *Arch. Biochem. Biophys.* **370**, 119–125.
- Pommier, Y., Pourquier, P., Fan, Y., and Strumberg, D. (1998). Mechanism of action of eukaryotic DNA topoisomerase I and drugs targeted to the enzyme. *Biochim. Biophys. Acta* **1400**, 83–105.
- Pritchard, D.M., Watson, A.J., Potten, C.S., Jackman, A.L., and Hickman, J.A. (1997). Inhibition by uridine but not thymidine of p53-dependent intestinal apoptosis initiated by 5-fluorouracil: evidence for the involvement of RNA perturbation. *Proc. Natl. Acad. Sci. USA* **94**, 1795–1799.
- Reden, J. (1990). Molsidomine. *Blood Vessels* **27**, 282–294.
- Rine, J., Hansen, W., Hardeman, E., and Davis, R.W. (1983). Targeted selection of recombinant clones through gene dosage effects. *Proc. Natl. Acad. Sci. USA* **80**, 6750–6754.
- Rittberg, D.A., and Wright, J.A. (1989). Relationships between sensitivity to hydroxyurea and 4-methyl-5-amino-1-formylisoquinoline thiosemicarbazone (MAIO) and ribonucleotide reductase RNR2 mRNA levels in strains of *Saccharomyces cerevisiae*. *Biochem. Cell Biol.* **67**, 352–357.
- Ruggero, D., and Pandolfi, P.P. (2003). Does the ribosome translate cancer? *Nat. Rev. Cancer* **3**, 179–192.
- Ruggero, D., Grisendi, S., Piazza, F., Rego, E., Mari, F., Rao, P.H., Cordon-Cardo, C., and Pandolfi, P.P. (2003). Dyskeratosis congenita and cancer in mice deficient in ribosomal RNA modification. *Science* **299**, 259–262.
- Schreiber, S.L., and Crabtree, G.R. (1992). The mechanism of action of cyclosporin A and FK506. *Immunol. Today* **13**, 136–142.
- Service, R.F. (2000). Biochemistry. Protein arrays step out of DNA's shadow. *Science* **289**, 1673.
- Soler, F., Plenge-Tellechea, F., Fortea, I., and Fernandez-Belda, F. (2000). Clomipramine and related structures as inhibitors of the skeletal sarcoplasmic reticulum Ca²⁺ pump. *J. Bionerg. Biomembr.* **32**, 133–142.
- Steinmetz, L.M., Scharfe, C., Deutschbauer, A.M., Mokranjac, D., Herman, Z.S., Jones, T., Chu, A.M., Giaever, G., Prokisch, H., Oefner, P.J., and Davis, R.W. (2002). Systematic screen for human disease genes in yeast. *Nat. Genet.* **31**, 400–404.
- Stocklein, W., and Piepersberg, W. (1980). Binding of cycloheximide to ribosomes from wild-type and mutant strains of *Saccharomyces cerevisiae*. *Antimicrob. Agents Chemother.* **18**, 863–867.
- Sugimoto, M., Kuo, M.L., Roussel, M.F., and Sherr, C.J. (2003). Nucleolar Arf tumor suppressor inhibits ribosomal RNA processing. *Mol. Cell* **11**, 415–424.
- Sun, C., and Woolford, J.L., Jr. (1994). The yeast NOP4 gene product is an essential nucleolar protein required for pre-rRNA processing and accumulation of 60S ribosomal subunits. *EMBO J.* **13**, 3127–3135.
- Tanayama, S., Nakai, Y., Fujita, T., Sukuoki, Z., Imashiro, Y., and Masuda, K. (1974). Biotransformation of molsidomine (N-ethoxycarbonyl-3-morpholinolinosyndonimine), a new antianginal agent in rats. *Xenobiotica* **4**, 175–191.
- Truan, G., Epinat, J.C., Rougeulle, C., Cullin, C., and Pompon, D. (1994). Cloning and characterization of a yeast cytochrome b5-encoding gene which suppresses ketoconazole hypersensitivity in a NADPH-P-450 reductase-deficient strain. *Gene* **142**, 123–127.
- Tunaru, S., Kero, J., Schaub, A., Wufka, C., Blaukat, A., Pfeffer, K., and Offermanns, S. (2003). PUMA-G and HM74 are receptors for nicotinic acid and mediate its anti-lipolytic effect. *Nat. Med.* **9**, 352–355.
- Venema, J., and Tollervey, D. (1999). Ribosome synthesis in *Saccharomyces cerevisiae*. *Annu. Rev. Genet.* **33**, 261–311.
- Volarevic, S., Stewart, M.J., Ledermann, B., Zilberman, F., Terracciano, L., Montini, E., Grompe, M., Kozma, S.C., and Thomas, G. (2000). Proliferation, but not growth, blocked by conditional deletion of 40S ribosomal protein S6. *Science* **288**, 2045–2047.
- Weir, I.E., Pham, N.A., and Hedley, D.W. (2003). Oxidative stress is generated via the mitochondrial respiratory chain during plant cell apoptosis. *Cytometry* **54A**, 109–117.
- White, T.C., Marr, K.A., and Bowden, R.A. (1998). Clinical, cellular, and molecular factors that contribute to antifungal drug resistance. *Clin. Microbiol. Rev.* **11**, 382–402.
- Wilson, I.D., Fromson, J.M., Illing, H.P., and Schraven, E. (1987). The metabolism of [¹⁴C]N-ethoxycarbonyl-3-morpholinolinosyndonimine (molsidomine) in man. *Xenobiotica* **17**, 93–104.
- Winzeler, E.A., Shoemaker, D.D., Astromoff, A., Liang, H., Anderson, K., Andre, B., Bangham, R., Benito, R., Boeke, J.D., Bussey, H., et al. (1999). Functional characterization of the *S. cerevisiae* genome by gene deletion and parallel analysis. *Science* **285**, 901–906.
- Yoshida, S., Ikeda, E., Uno, I., and Mitsuzawa, H. (1992). Characterization of a staurosporine- and temperature-sensitive mutant, stt1, of *Saccharomyces cerevisiae*: STT1 is allelic to PKC1. *Mol. Gen. Genet.* **231**, 337–344.
- Ziauddin, J., and Sabatini, D.M. (2001). Microarrays of cells expressing defined cDNAs. *Nature* **411**, 107–110.